NANO LETTERS

2009
Vol. 9, No. 2
814-818

Graphene-based Composite Thin Films for Electronics

Goki Eda and Manish Chhowalla*

Rutgers University, Materials Science and Engineering, Piscataway, New Jersey 08854

Received November 21, 2008; Revised Manuscript Received January 4, 2009

ABSTRACT

The electrical properties of solution-processed composite thin films consisting of functionalized graphene sheets (FGS) as the filler and polystyrene (PS) as the host material are described. We demonstrate that transistors from graphene-based composite thin films exhibit ambipolar field effect characteristics, suggesting transport via percolation among FGS in the insulating PS matrix. Device characteristics as a function of the FGS size are also reported. The results indicate that devices fabricated using the largest size FGS yield the highest mobility values. This simple and scaleable fabrication scheme based on a commodity plastic could be useful for low-cost, macro-scale electronics.

Graphene-based composites are emerging as new class of materials that hold promise for several applications.[1] Graphene, a single sheet of graphite, possesses extraordinary electrical, thermal, and mechanical properties arising from its unique structure.[2] When incorporated into polymer[3−6] or ceramic[7] matrices, these properties manifest as remarkable improvements in the host material. Graphene-based polymer composites exhibit extraordinarily low electrical percolation threshold (0.1 vol %) due to large conductivity and aspect ratio of the graphene sheets (atomic thickness and micrometer-sized lateral dimensions).[3,6] The mechanical and thermal properties of these materials rank among the best in comparison with other carbon-based composites due to strong interactions between polymer hosts and graphene sheets.[1,5] The highly conductive nature of graphene and ease of incorporation into polymers and ceramics has also opened up the possibility of their use as transparent conductors.[7] Furthermore, we recently demonstrated that atomically sharp edges of graphene incorporated into a PS host can be exploited for field emission.[8]

Graphene is a zero band gap semiconductor exhibiting large electric field effect,[9] allowing doping with electrons or holes via electrostatic gating. The fact that graphene does not have a band gap poses a challenge for digital applications, but its high mobility is attractive for high frequency analog electronics or spintronics.[10,11] The semiconducting and robust mechanical properties of reduced graphene have been exploited for macro-scale thin film electronic devices[12,13] and high performance resonators.[14] Semiconducting behavior has yet to be demonstrated in graphene-based composites. The compatibility of graphene with polymers and ceramics opens up a route toward realization of semiconducting composite materials from electrically passive host materials. That is, introduction of percolating graphene network within an insulating material may render it semiconducting. In this study, we show that incorporation of functionalized graphene sheets (FGS) in polystyrene (PS) matrix results in composite thin films that are semiconducting and exhibit ambipolar field effect. These composites can be deposited uniformly over large areas in the form of thin films from solution onto which devices can be fabricated without extensive lithography. The reported solution-based approach for fabricating thin film transistors (TFTs) from FGS and PS could bring a new dimension to the potential applications of graphene-based composites.

The scheme for fabricating graphene-based polymer composites proposed by Stankovich et al.[3] utilizes the chemical versatility of graphene oxide (GO), a solution processable precursor to graphene. GO is hydrophilic and disperses mainly in aqueous media but can be chemically functionalized with isocyanate to make it soluble in organic solvents such as dimethylformamide (DMF),[15] which is commonly used to dissolve many polymers. After dissolving the functionalized GO with a polymer in a solvent, it can be reduced to form a FGS-polymer solution.

The semiconducting graphene-based composite thin films were prepared by the method outlined by Stankovich et al.[15] Initially, graphite oxide was prepared using the modified Hummers method[16] and functionalized using phenyl isocyanate and dispersed in DMF at a concentration of 1.5 mg/mL. Linear monodisperse PS (25.3 mg) (molecular weight = 2 043 000 g/mol, Scientific Polymer Products Inc.) was added to 10 mL of functionalized GO dispersion in DMF and stirred at 60 °C until completely dissolved. A solution consisting of 10% volume fraction of FGS in PS was prepared. To reduce functionalized GO, dimethyhydrazine was added to the solution at a concentration of 1 vol % and

* To whom correspondence should be addressed. E-mail: manish1@rci.rutgers.edu.

10.1021/nl8035367 CCC: $40.75 © 2009 American Chemical Society
Published on Web 01/27/2009

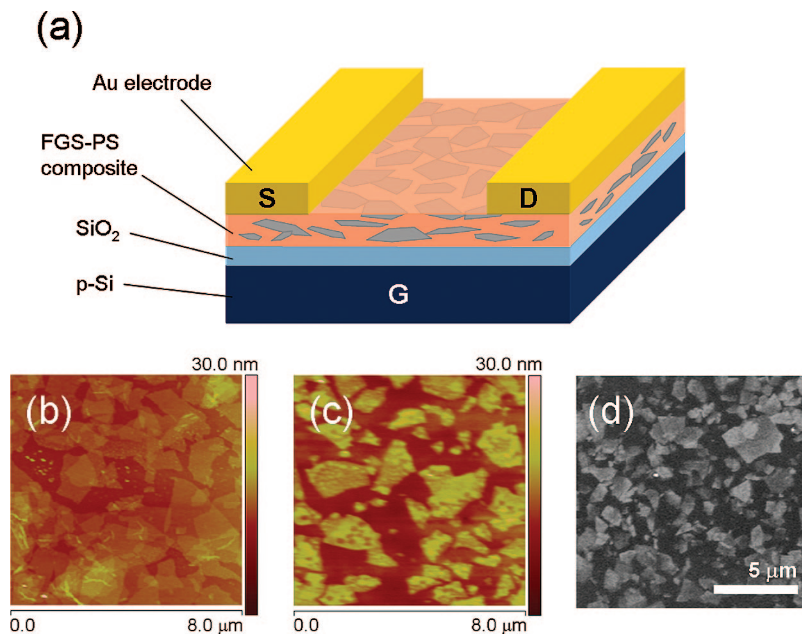

Figure 1. (a) Schematic of FGS-PS composite thin film field effect devices. (b) AFM of (b) phenyl-isocyanate treated GO and (c) FGS-PS composite thin films. (d) SEM of typical as-deposited FGS-PS composite thin films. Contrast can be seen between conductive FGS (light) and insulating PS matrix (dark).

the mixture was allowed to stand for 24 h at 80 °C. The solution obtained thus was spin-coated on degenerately doped Si substrates with 300 nm thermal oxide at 1000−4000 rpm to obtain uniform thin films with thickness of 14−30 nm. The samples were then baked at 200 °C to remove residual solvent and dimethylhydrazine. Spin-coating and baking were carried out in a glovebox to avoid coagulation of polystyrene due to moisture. Gold source (S) and drain (D) electrodes were thermally evaporated on composite thin films for transport measurements. The Si substrate was used as the gate (G) electrode. Devices with channel lengths ranging from 14 to 230 μm and channel width of 400 μm were tested. The transport measurements were conducted in a cryostat (ST-500, Janis) with a base pressure of 10^{-5} Torr at temperatures ranging from 4.2 and 370 K. The device structure is schematically shown in Figure 1a. The size of FGS was found to remain unchanged during the reduction and deposition processes (Figure 1b,c). The size of FGS is dependent on the size of initial graphite crystals but can be adjusted by ultrasonication of the suspension to break up the individual sheets.[17] In this study, composite thin films consisting of FGS with three different average sizes were prepared from two graphite sources (Bay Carbon Inc. and Branwell Graphite Ltd.). Because of viscous flow of polymer solution during spin-coating, most FGS were found to be lying nearly parallel to the substrate surface (Figure 1c). Some FGS were nearly exposed at the composite surface as indicated by the higher contrast against the insulating matrix in the scanning electron micrograph (SEM) (Figure 1d).

The composite thin films were electrically conducting with the sheet resistance being on the order of 1∼10 MΩ/□ due to percolation among the FGS within the PS matrix. The corresponding conductivity values for the thin films ranged from 1 to 24 S/m, which is in agreement with the values reported for bulk composites.[3] Conductance modulation by bottom-gating was observed in all measured devices and showed ambipolar field effect similar to reduced GO thin film transistors.[12,18] Field effect mobility was generally higher for holes than for electrons by a factor of about 2∼5 and was generally between 0.1 and 1 cm^2/Vs in ambient conditions. Unlike reduced GO, the composite devices were weakly sensitive to unintentional ambient doping, suggesting that majority of FGS responsible for the carrier transport are embedded within the PS. The minima in the transfer characteristic curves were readily visible at threshold voltages of around +20 V that shifted to +16 V when measurements were performed in vacuum (Figure 2a). At low temperatures in vacuum, the threshold voltage (V_{th}) remained near V_g = 0 V and the hysteresis resulting from upward and downward sweeps of the gate voltage was found to be minimal (Figure 2b). The temperature dependent transfer characteristics in Figure 2c indicate that the on/off ratio of the devices increases with decreasing temperature, a trend that has also been observed for individual monolayer of reduced GO.[18] The on/off ratio with temperature trend observed for FGS-PS thin films suggests that the FGS are well dispersed and remain exfoliated in the PS matrix. The $I_{sd}-V_{sd}$ characteristics of the devices were linear even at 4.2 K, indicating negligible energy barriers at the contacts (Figure 2d).

To study the device characteristics with film thickness, the spin coating speed was varied. The device resistance increased with decreasing film thickness (i.e., increasing spin-coating speed during deposition) as expected. However, the qualitative features of the transfer characteristics remained largely unchanged (Figure 2e). The on/off ratio did not vary significantly with film thickness indicating that electrostatic screening effects are not critical for the studied thickness range (Figure 2e, inset). These results suggest that our composite thin films consist of nearly one monolayer of graphene sheet along the thickness in the z-direction. It is

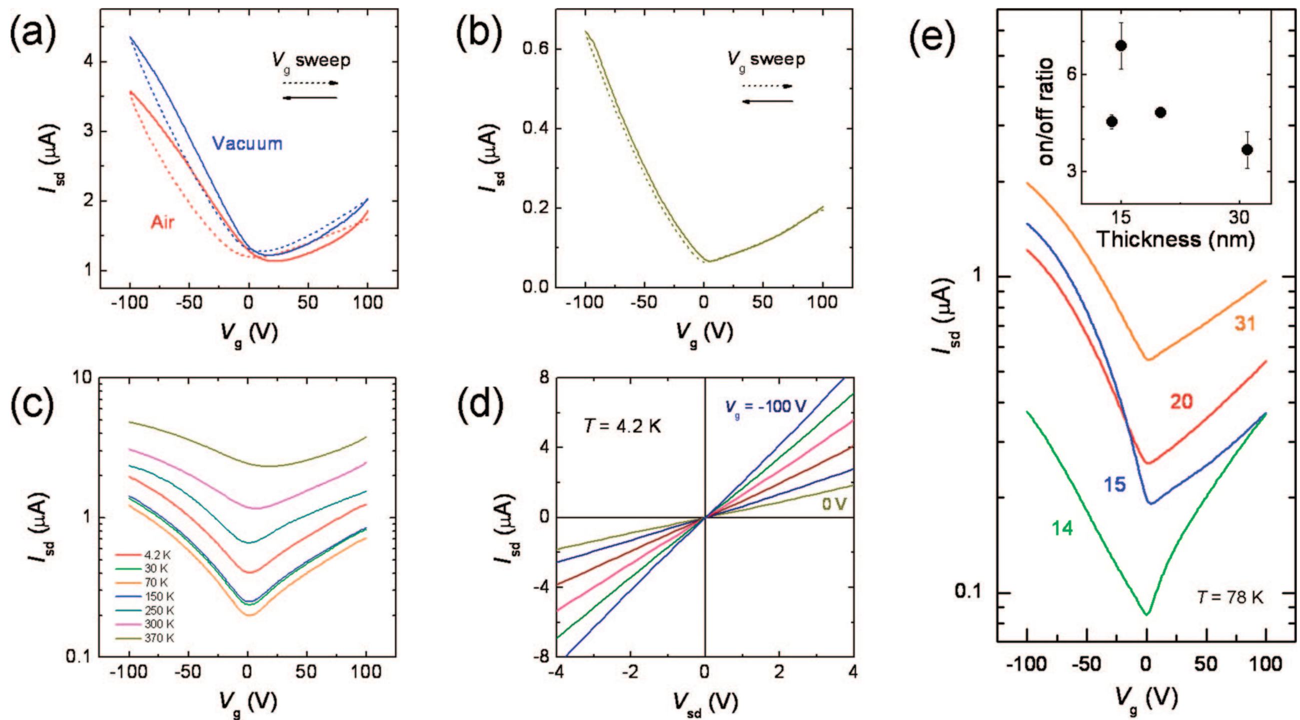

Figure 2. (a) Transfer characteristics of a FGS-PS composite thin film in air and vacuum. Hysteresis from different sweep directions of V_g (V_{sd} = 1 V) are shown. Transfer characteristics (b) at 90 K in linear scale and (c) at various temperatures in log scale (V_{sd} = 1 V). (d) $I_{sd}-V_{sd}$ characteristics with different V_g measured at 4.2 K. (e) Transfer characteristics of thin films with different film thicknesses (indicated in nanometers) measured at 78 K. The inset shows the on/off ratio as a function of film thickness.

also worth noting that the device properties remained consistent before and after cooling down to liquid helium temperature. Atomic force microscope (AFM) analysis revealed that the material did not crack or change its morphology upon lowering of temperature. This observation may suggest that FGS provides structural rigidity to PS against deformation and crack propagation.

The thin film conductance as a function of temperature (from 4.2 to 370 K) was measured and shown in Figure 3a. The conductance decreased with decreasing temperature down to about 50 K and increased slightly with further lowering of temperature. Such anomalous behavior has been observed previously in graphitic flakes[19] and reduced graphene oxide thin films.[12] It is likely that at temperatures below 50 K, electron−phonon scattering limits the carrier transport. Above 250 K, the temperature dependence can be fitted with a thermal activation model, yielding an activation energy of 87 meV for transport. The FGS-PS composite is a highly disordered system as FGS contain intrinsic defects and are randomly arranged within PS. Therefore, the description of carrier transport through the composite is expected to require a combination of models. That is, there are contributions from thermal activation of carriers, tunneling through PS matrix, and variable range hopping both within and between the FGS.[18] The activation energy obtained above is only a rough estimation of the total energy required for thermal carrier activation and transport.

Further insight into the transport mechanism can be achieved by separating these contributions. The conductivity of the material is expressed as $\sigma = e(n_e\mu_e + n_h\mu_h)$ where e is the electron charge, n is the carrier concentration, μ is the carrier mobility, and the subscripts indicate the two charge carrier types, electrons and holes. The mobility for each type of carriers can be extracted from the two branches of the transfer characteristics using $\mu = (L/WC_{ox}V_{sd})g_m$ where L and W are the channel length and the width, C_{ox} is the gate oxide capacitance, V_{sd} is the source-drain voltage, and g_m is the transconductance. Further, the intrinsic carrier concentration (n) can also be calculated by assuming that $n_e = n_h = n$ at the minimum conductivity point.[20] The hole and electron mobility and the intrinsic carrier concentration obtained thus are plotted as a function of temperature in Figure 3b,c. This analysis reveals that μ and n follow different temperature dependences. The carrier mobility decreases rapidly with increasing temperature up to about 60 K and gradually increases with further increase in temperature. The intrinsic carrier concentration shows similar but more gradual changes below 250 K and then rapidly increases above this temperature. The Arrehenius fit for n above 250 K yields an activation energy of 56 meV, which corresponds to the energy required to activate carriers from defects and doping states. The dopant type can be identified from the threshold voltage shift in the transfer characteristics. For example, positive threshold voltages indicate p-type doping since negative charge carriers must be induced by positive bias to neutralize the excess holes, and vice versa for negative threshold voltages. The device is nearly neutral up to 250 K but becomes increasingly hole-doped above this temperature. This behavior indicates that thermal activation of hole carriers in this temperature regime dominates the transport properties.

The carriers injected into FGS-PS composite thin films must be transported through and between FGS. The carrier

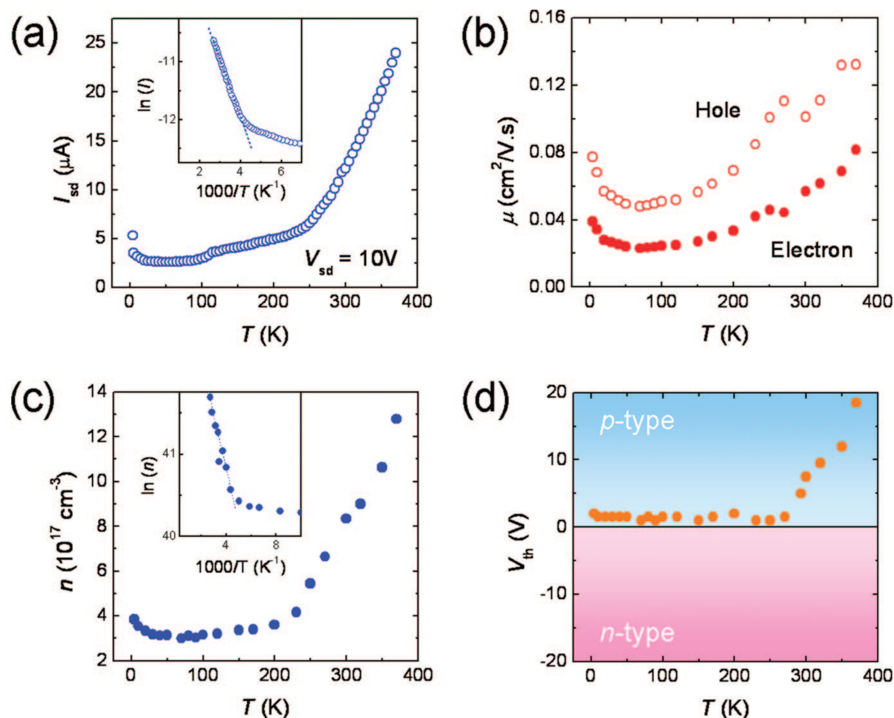

Figure 3. (a) Temperature dependence of source-drain current (I_{sd}) with V_{sd} = 10 V and floating gate. The current values were recorded for increasing temperatures from 4.2 up to 370 K. The inset shows the corresponding Arrhenius plot. (b) The electron and hole mobilities, (c) intrinsic carrier concentration, and (d) threshold voltage as a function of temperature.

mobility may be limited by defects within each FGS and energy barriers at sheet-to-sheet junctions. To gain insight into the effect of sheet-to-sheet junctions, we examined field effect devices fabricated from FGS with three different average sizes (S_{ave}) ranging from 0.44 to 24 μm and three different channel lengths (L) ranging from 14 to 230 μm while other parameters were kept constant. The distribution of the flake sizes are shown in Figure 4a−c. The devices were found to have uniform conductivity irrespective of the channel length as expected for a system well above the percolation threshold. The field effect mobilities are plotted as a function of a nondimensional length scale, S_{ave}/L, as in Figure 4d. The results indicate that the mobility is weakly dependent on flakes size and nearly independent of channel length partly similar to the results previously reported for percolating networks of carbon nanotubes.[21] When the channel length was kept constant, the mobility typically increased with increasing FGS size suggesting that sheet-to-sheet junction is limiting the mobility. The highest electron and hole mobilities of 0.2 and 0.7 cm²/V•s, respectively, were found for FGS composite devices with average flake sizes of 24 μm. This suggests that increasing the average size of FGS may be a key to enhancing the device performance. Another route for improving the device performance is to optimize the reduction conditions[22] for FGS thereby reducing the defects in the material. Since the typical mobility values reported for reduced GO is ∼ 1 −10 cm²/V•s,[12,20] there is room for further improvement.

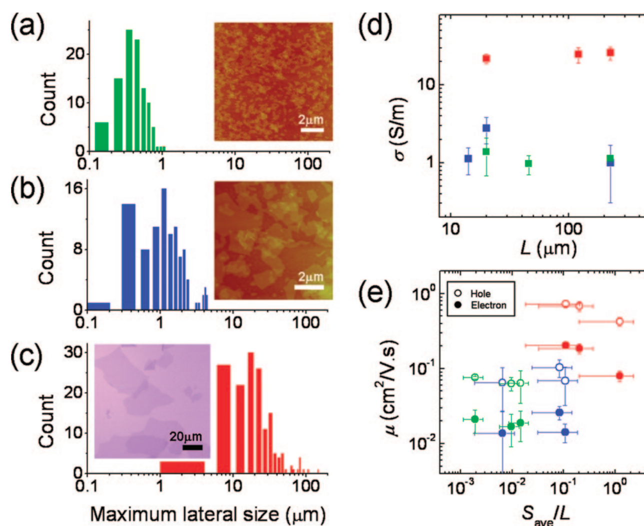

Figure 4. (a) Size distribution of FGS produced from graphite obtained from Bay Carbon Inc. and ultrasonicated for 10 h. (b) Same as panel a but without ultrasonication. The insets of panels a and b show the AFM image of FGS corresponding to these size distributions (c) Size distribution of FGS produced from graphite obtained from Branwell Graphite Ltd. Inset: optical micrograph of FGS corresponding to this size distribution. The average flake size (S_{ave}) for panels a, b, and c are 0.44, 1.5, and 22.4 μm, respectively. (d) Device conductivities measured in ambient conditions as a function of channel length. (e) Field effect mobilities as a function of nondimensional length scale, S_{ave}/L. The color of symbols in panels d and e represents different flake size distribution and corresponds to those of panels a–c.

In summary, a solution-processable semiconducting thin film composite consisting of FGS and PS exhibiting ambipolar transfer characteristics has been described. The FGS are well dispersed and percolating within the PS matrix, giving rise to electrical properties similar to individual monolayer of reduced GO and its thin films. The material is intrinsically hole-doped at room temperature and becomes

increasingly p-type at higher temperatures. The carrier mobilities are limited by the disorder of each FGS and the sheet-to-sheet junctions. Further optimization of material parameters and reduction conditions are expected to result in better performing devices, rivaling organic counterparts. The reported scheme for fabricating semiconducting composite thin films from graphene and a commodity plastic could be useful for low-cost, macroscale thin film electronics.

Acknowledgment. This work was funded by the National Science Foundation CAREER Award (ECS 0543867).

References

(1) Ramanathan, T.; Abdala, A. A.; Stankovich, S.; Dikin, D. A.; Herrera-Alonso, M.; Piner, R. D.; Adamson, D. H.; Schniepp, H. C.; Chen, X.; Ruoff, R. S.; Nguyen, S. T.; Aksay, I. A.; Prud'Homme, R. K.; Brinson, L. C. *Nat. Nanotechnol.* **2008**, *3*, 327–331.

(2) Geim, A. K.; Novoselov, K. S. *Nat. Mater.* **2007**, *6* (3), 183–191.

(3) Stankovich, S.; Dikin, D. A.; Dommett, G. H. B.; Kohlhaas, K. M.; Zimney, E. J.; Stach, E. A.; Piner, R. D.; Nguyen, S. T.; Ruoff, R. S. *Nature* **2006**, *442* (7100), 282–286.

(4) Verdejo, R.; Barroso-Bujans, F.; Rodriguez-Perez, M. A.; de Saja, J. A.; Lopez-Manchado, M. A. *J. Mater. Chem.* **2008**, *18*, 2221–2226.

(5) Yu, A.; Ramesh, P.; Itkis, M. E.; Bekyarova, E.; Haddon, R. C. *J. Phys. Chem. C* **2007**, *111* (21), 7565–7569.

(6) Liu, N.; Luo, F.; Wu, H.; Liu, Y.; Zhang, C.; Chen, J. *Adv. Funct. Mater* **2008**, *18*, 1518–1525.

(7) Watcharotone, S.; Dikin, D. A.; Stankovich, S.; Piner, R.; Jung, I.; Dommett, G. H. B.; Evmenenko, G.; Wu, S. E.; Chen, S. F.; Liu, C. P.; Nguyen, S. T.; Ruoff, R. S. *Nano Lett.* **2007**, *7* (7), 1888–1892.

(8) Eda, G.; Unalan, H. E.; Rupesinghe, N.; Amaratunga, G.; Chhowalla, M. *Appl. Phys. Lett.* **2008**, *93*, 233502.

(9) Novoselov, K. S.; Geim, A. K.; Morozov, S. V.; Jiang, D.; Zhang, Y.; Dubonos, S. V.; Grigorieva, I. V.; Firsov, A. A. *Science* **2004**, *306* (5696), 666–669.

(10) Hill, E. W.; Geim, A. K.; Novoselov, K.; Schedin, F.; Blake, P. *IEEE Trans. Magn.* **2006**, *42* (10), 2694.

(11) Tombros, N.; Jozsa, C.; Popinciuc, M.; Jonkman, H. T.; van Wees, B. J. *Nature* **2007**, *448* (7153), 571–574.

(12) Eda, G.; Fanchini, G.; Chhowalla, M. *Nat. Nanotechnol.* **2008**, *3*, 270–274.

(13) Robinson, J. T.; Perkins, F. K.; Snow, E. S.; Wei, Z.; Sheehan, P. E. *Nano Lett.* **2008**, *8* (10), 3137–3140.

(14) Robinson, J. T.; Zalalutdinov, M.; Baldwin, J. W.; Snow, E. S.; Wei, Z.; Sheehan, P.; Houston, B. H. *Nano Lett.* **2008**, *8* (10), 3441–3445.

(15) Stankovich, S.; Piner, R.; Nguyen, S. T.; Ruoff, R. S. *Carbon* **2006**, *44* (15), 3342–3347.

(16) Hirata, M.; Gotou, T.; Horiuchi, S.; Fujiwara, M.; Ohba, M. *Carbon* **2004**, *42* (14), 2929–2937.

(17) Sun, X.; Liu, Z.; Welsher, K.; Robinson, J. T.; Goodwin, A.; Zaric, S.; Dai, H. *Nano Res.* **2008**, *1*, 203–212.

(18) Gomez-Navarro, C.; Weitz, T. R.; Bittner, A. M.; Scolari, M.; Mews, A.; Burghard, M.; Kern, K. *Nano Lett.* **2007**, *7* (11), 3499–3503.

(19) Zhang, Y.; Small, J. P.; Pontius, W. V.; Kim, P. *Appl. Phys. Lett.* **2005**, *86*, 073104.

(20) Wang, S.; Chia, P.-J.; Chua, L.-L.; Zhao, L.-H.; Png, R.-Q.; Sivaramakrishnan, S.; Zhou, M.; Goh, R. G.-S.; Friend, R. H.; Wee, A. T.-S.; Ho, P. K.-H. *Adv. Mater.* **2008**, *20*, 3440–3446.

(21) Hur, S. H.; Kocabas, C.; Gaur, A.; Park, O. O.; Shim, M.; Rogers, J. A. *J. Appl. Phys.* **2005**, *98* (11), 114302.

(22) Jung, I.; Dikin, D. A.; Piner, R. D.; Ruoff, R. S. *Nano Lett.* **2008**, *8* (12), 4283–4287.

NL8035367